LA-UR-16-27365
Approved for public release; distribution is unlimited.

Title: Progress on FP13 Total Cross Section Measurements Capability

Author(s): Ullmann, John Leonard
Couture, Aaron Joseph
Koehler, Paul E.
Mocko, Michal
Mosby, Shea Morgan
Wender, Stephen Arthur

Intended for: Report

Issued: 2016-09-26

Progress on FP13 Total Cross Section Measurements Capability

J.L. Ullmann, P.E. Koehler, A. Couture, M. Mocko, S. Mosby, S.A. Wender
P-27, Los Alamos National Laboratory

I. INTRODUCTION

An accurate knowledge of the neutron capture cross section is important for many applications, both within the weapons program and in other fields. Experimental measurements are important since theoretical calculations of capture have been notoriously difficult, with the ratio of measured to calculated cross sections often a factor of 2 or more in the 10 keV to 1 MeV region. However, a direct measurement of capture cannot be made on many interesting radioactive nuclides because of their short half life or backgrounds caused by their nuclear decay. On the other hand, neutron transmission measurements of the total cross section are feasible for a wide range of radioactive nuclides since the detectors are far from the sample, and often are less sensitive to decay radiation. The parameters extracted from a total cross section measurement, which include the average resonance spacing, the neutron strength function, and the average total radiation width, $\langle\Gamma_\gamma\rangle$, provide tight constraints on the calculation of the capture cross section, and when applied produce much more accurate results.

It was pointed out by Koehler, et al. (LA-UR-14-21656) that these measurements can be made using the intense epithermal neutron flux at the Lujan Center on relatively small quantities of target material. It was the purpose of this project to investigate and develop the capability to make these measurements. A great deal of progress was made towards establishing this capability during 2016, but more work remains to be done.

II. PROGRESS IN FY16

A. Flight Path

Flight-path 13 views the second-tier cold moderator at the Lujan Center. It was originally configured to transport thermal and cold neutrons to 65 m using evacuated neutron guides. The guide centerline was displaced 0.5719 degree from the zero-degree line so that higher-energy neutrons (above about 0.1 eV) were not transported. Since the "high energy" neutrons were needed for these measurements, the beam line was straightened. This was accomplished by sliding the first 20 m of the guide back to the zero-degree line. The next 15 meters of the guide was moved completely out of the zero-degree path by replacing the positioning sliders with longer sliders while using the existing support structures. The last 15 m of the guide was already far enough from the zero-degree line to allow new vacuum pipes to be installed.

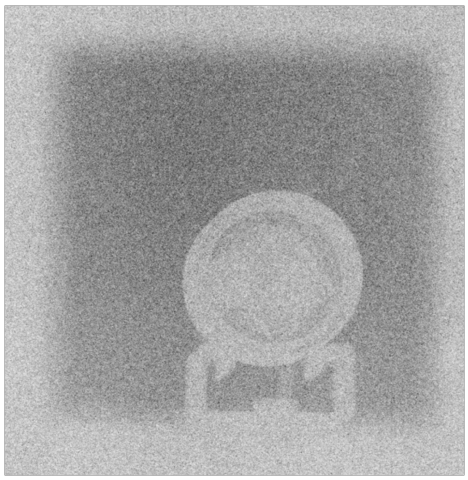

FIG. 1. Image of one-inch diameter LiI detector coupled to a two-inch diameter phototube mounted on the detector stand. The image was taken with a "white" image plate using the 6 mm collimator. Note the beam image, which is about 13 cm X 13 cm, is a pin-hole image of the moderator.

A steel collimator assembly was installed in the existing guide gap at about 30 m, and brass collimator inserts were used to define the beam spot. The sample was placed immediately downstream of the collimator inserts. Inserts with aperture diameters of 6 mm and 1 mm were used. New 8-in diameter evacuated beam pipes were installed downstream of the collimator, but only the first 15 m section arrived in time to be used for the test runs. A thin lithium-plastic sheet was placed upstream of the collimator to limit the low energy neutrons hitting the collimator and being transported to the detectors.

Figure 1 shows an image of the beam at the wall behind the detector location, at about 67 meters, with the one-inch diameter LiI detector mounted on the detector stand. The 6 mm collimator was used. Figure 2 shows the steel collimator shell with brass inserts located at 30 m, looking upstream. Additional concrete block and polyethylene shielding surrounds the collimator assembly.

B. Data Acquisition System

A data acquisition system based on the CAEN VX1730B digitizer with "PSD" firmware was developed. The system recorded the time, short-gate pulse integral and long-gate pulse integral for each detector event. For the CLYC detector, these two integrals are used for pulse-

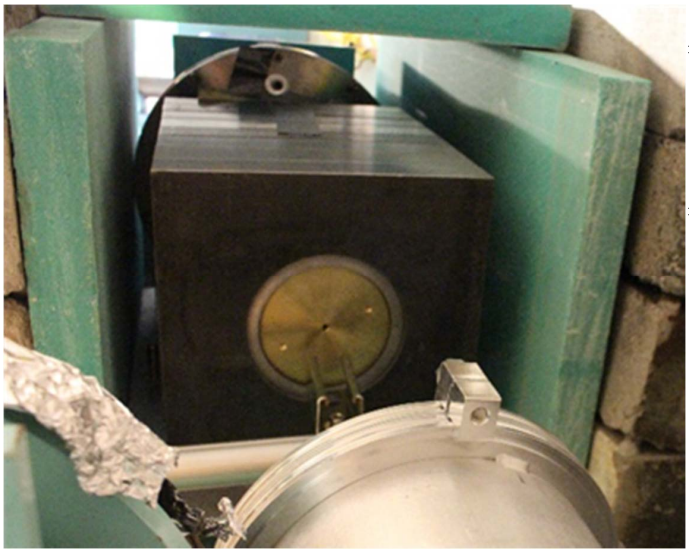

FIG. 2. The square steel collimator shell and brass inserts with 6 mm aperture located at approx. 30 m, looking upstream. Borated polyethylene and concrete block shielding surround the steel plates.

TABLE I. Digitizer Parameters

Detector	Channel	Short Gate	Long Gate
CLYC	5	120 ns	640 ns
LiGlass	3	100 ns	500 ns
LiI	4	100 ns	500 ns

shape discrimination ("PSD"). The parameters for each detector are shown in Table I. In addition, the beam To time and the proton current monitor "v to f" signal were also recorded.

C. Detectors

Three different detectors were borrowed and tested, all mounted with phototubes "end on" and thus in the neutron beam. The detector parameters are shown in Table II. The first detector was a LiI crystal. This detector had reasonable efficiency and timing, but I has a total cross section with many resonances in the energy region of interest. The second detector was a Cerium-doped "CLYC" crystal (Cs_2LiYCl_6). CLYC has neutron-gamma pulse-shape discrimination (PSD) capabilities. Although the Cs in CLYC also has resonances in the region of interest, especially at 5.91 and 22.51 eV, they seemed less intrusive than in the LiI, and the gamma-ray discrimination properties may be very advantageous. Finally, a Li glass detector was tested. This detector saturated at high count rates in the "gamma-flash" time of flight region (less than 50 μsec) and was sensitive to gamma rays out to long times. However, it has higher efficiency to neutrons than CLYC, contains no nuclides with strong resonances in the eV to keV region, and is considerably less expensive.

TABLE II. Detector Parameters

	Diameter (cm)	Thickness (cm)	^{6}Li/cm^2	Area (cm^2)
CLYC	2.54	1.0	1.08 X 10^{22}	5.1
LiGlass	12.5	1.5	2.01 X 10^{22}	123.
LiI	2.54	0.15	1.09 X 10^{22}	5.1

FIG. 3. Li-glass detector mounted at 65 m in FP-13.

Figure 3 shows the Li-glass detector mounted at 65 m in FP13.

III. RESULTS OF TESTS WITH BEAM

During Feb., 2016, tests were made with beam to assess the performance of the different detectors and to evaluate the characteristics of the flight path. The beam flux was measured with each detector, and a simple "target-in/target-out" total cross section measurement was made using a 90 mg/cm^2 metallic ^{169}Tm foil and the Li-glass detector.

A. Moderator Function

The first step was to calibrate the flight path length by fitting the time of flight to known ^{169}Tm resonances. The measured time of flight includes an energy-dependent "moderation time" which must be determined. Although this could be done directly from the TOF data with care-

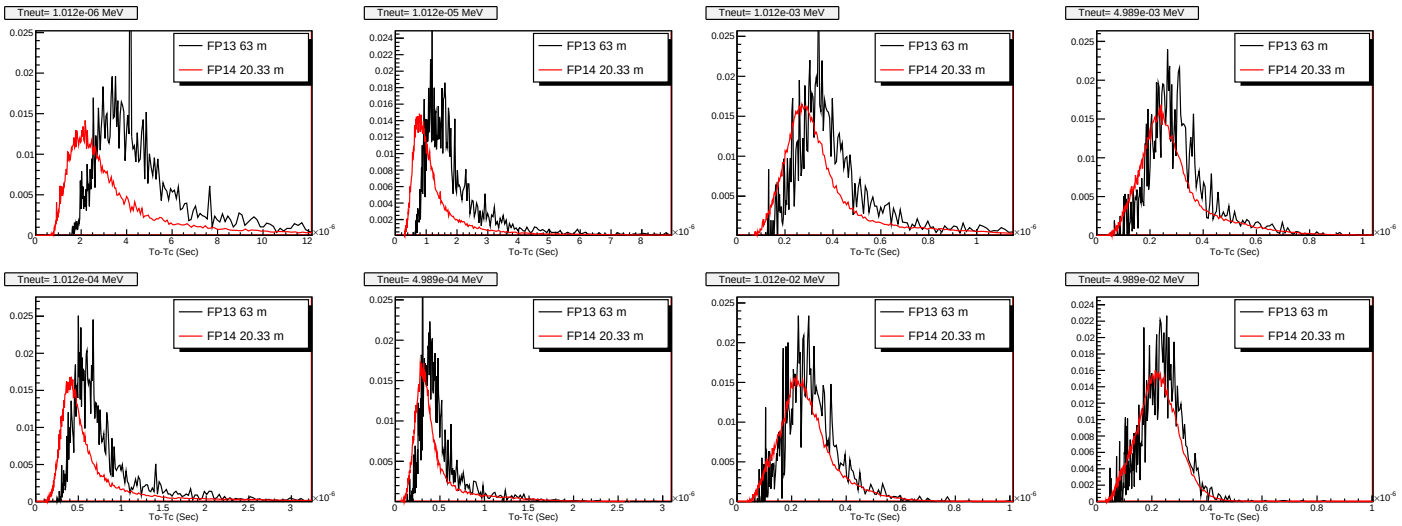

FIG. 4. Moderator function calculated for FP13 and FP14 for energies less than 1 keV.

FIG. 5. Moderator function calculated for FP13 and FP14 for energies greater than 1 keV.

ful peak fitting, we determined it from MCNP calculations done by Mocko. The calculated moderator functions are shown in Fig 4 for kinetic energies $T_{neut} \leq 1$ keV and in fig. 5 for $T_{neut} \geq 1$ keV. The functions are plotted a a function of the time difference T-T_c, where T_c is the kinematic time of flight and T is the measured time of flight. The figure compares the moderator functions calculated for Flight Path 13 and Flight Path 14. They are similar in shape, but displaced in time. The peak of the function was taken as the moderation time. For FP13 this corresponds to

$$\Delta T(\mu sec) = 0.2 + 3.3/\sqrt{E(eV)} \qquad (1)$$

Using this time, the measured time of flight is

$$TOF(\mu sec) = \frac{(72.3)(64.67m)}{\sqrt{E(eV)}} - 0.66 + \Delta T \qquad (2)$$

where the flight path length (64.67 m) and time intercept (-0.66 sec) were determined from a linear fit to the measured times of flight to the resonance energies.

B. Neutron flux

The neutron flux is determined by

$$\Phi(\epsilon) = \frac{N(\epsilon)}{T_0 d\epsilon} \frac{1}{AB\sigma(\epsilon)} \qquad (3)$$

where Φ is in n/cm^2/eV/T_0, N(ϵ) is the number of counts, dϵ is the width of the energy bin, σ is the ^{6}Li(n,t) cross section from ENDF/B-VI, A is the area of the detector, and B is the number of ^{6}Li atoms/cm^2. The area is taken from Table II except for the Li-glass detector,

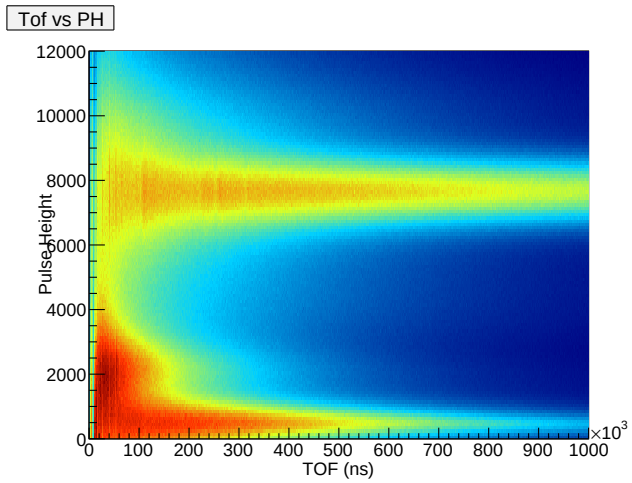

FIG. 6. Pulse integral (in digitizer units) vs time of flight for the Li-glass detector. The ^{6}Li(n,t) band, at a pulse height of about 7500 units, is obvious.

where the area is mutiplied by 0.5 to approximately account for the beam/detector overlap.

For the LiI and LiGl detectors, counts were determined subject to a gate around the pulse height of ^{6}Li(n,t) reaction (Q=4.78 MeV). The band for this reaction is clearly seen in the 2D Pulse Height (integral) vs time-of-flight spectrum shown in Fig. 6. Although the gate is intended to eliminate gammas detected in the scintillator, they are not completely eliminated, and the ^{6}Li peak sits on a gamma ray background which varies with neutron energy. This is illustrated in Fig 7 which shows the pulse height spectrum for the lithium glass detector in 5% energy bins at three neutron energies.

The CLYC detector has neutron-gamma pulse-shape discrimination capability. This is realized by comparing

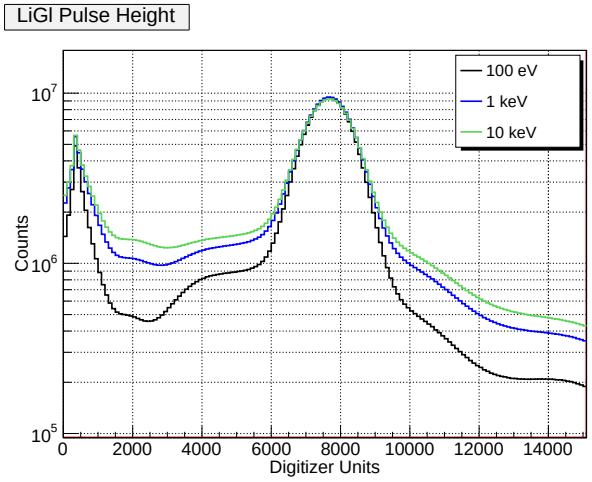

FIG. 7. Pulse "height" (area) in digitizer units spectrum for the Li-glass detector plotted in 5% energy bins at several neutron energies. The curves were normalized to the same maximum height.

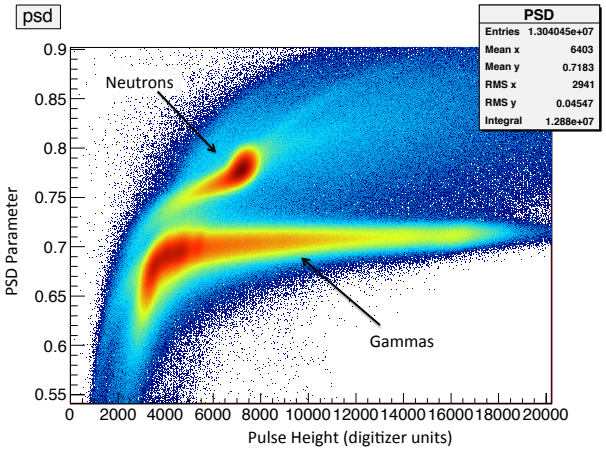

FIG. 8. The PSD parameter for the CLYC detector plotted against the total pulse height. The neutron and gamma-ray regions are indicated. Neutrons are detected by the ^{6}Li(n,t) reaction.

the integral of the detected waveform in a long and short time gate, as shown in Table I. The PSD parameter is the area of the waveform "tail" (tail = long gate - short gate) divided by the long gate area, as shown in Fig 8. The PSD gate for neutrons is set at 0.75. The pulse-height vs TOF spectrum gated by neutron PSD is shown in Fig 9. Gating on both spectra results in a much cleaner time of flight spectrum for the CLYC than the Li-glass or LiI detectors.

Note that the count rate as a function of time of flight for a neutron flux $\Phi \sim 1/\epsilon$ and cross section $\sigma \sim 1/\epsilon^{1/2}$, is flat between the resonances, and this should be expected in these measurements. The effect of the gamma-ray background in the Li-glass detector is obvious in the time of flight spectra shown in Fig 10, where the spectrum is definitely decreasing with time.

The flux calculated from eq. 3 is shown in Fig. 11. Also shown are MCNP calculations by Mocko for a fully-evacuated flight path and also for the case of having the last 15 m of the flight path in air, as was the case for this measurement. The calculations included the Al vacuum windows and Li-plastic absorber. The absolute values determined from the different detectors are roughly comparable, with the normalization differences perhaps due to inexact knowledge of the ^{6}Li density in each detector. The energy dependence of the Li-glass detector is very different from the others, and clearly shows the effects of high count rate and gamma background at the high energies, where the dips due to Al resonances at 34 and 88 keV are not observed. In addition, the measured cross section drops off at the 240 keV resonance in the ^{6}Li(n,t) cross section, most likely due to dead-time effects caused by the very high count rate at the resonance.

A simple test transmission measurement was made using a 90 mg/cm^2 ^{169}Tm target and the 6 mm collimator. For this measurement, the sample was "in" for about

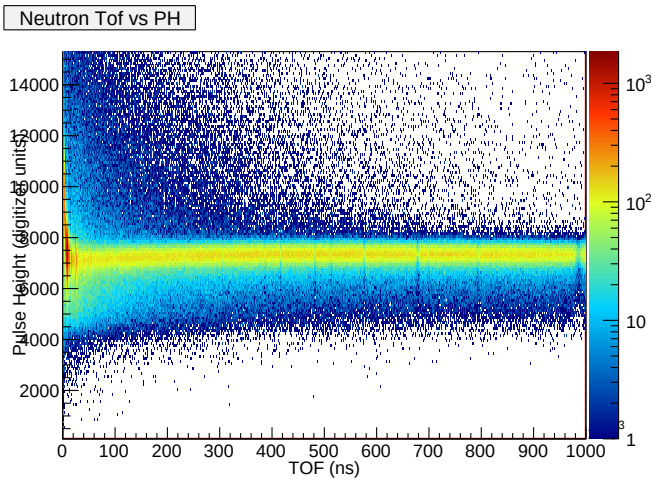

FIG. 9. Time of flight vs. pulse height, subject to neutron PSD gate, for the CLYC detector.

12 hours, and then "out" for 12 hours. Transmission is the ratio of "in"/"out" count rates, normalized by the integrated proton beam current. The measured values are compared to calculations made using the R-matrix SAMMY code and resonance parameters from ENDF/B-VI. SAMMY calculates the cross section from the resonance parameters and then broadens it with the moderator function and Doppler broadening. These calculations require a moderator function as a function of neutron energy. This was determined using the analytic "NTOF" form in SAMMY and fitting the parameters to the calculated moderator function shown in Figs 4 and 5. The fits were made to the calculated functions for FP14 instead of FP13, but as shown above, they are very similar in the

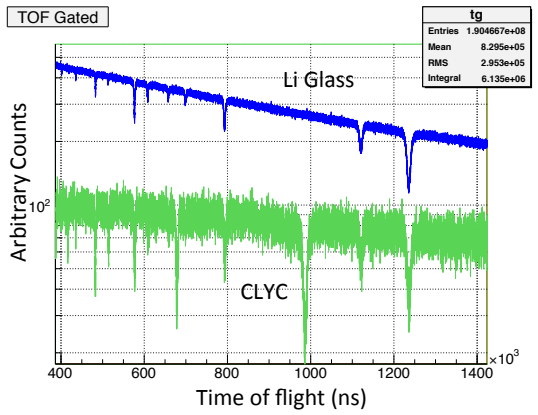

FIG. 10. Transmission spectrum for ^{169}Tm in the 400 to 1400 μsec (138 to 11 eV) range. The spectrum from the Li Glass and the CLYC detector are indicated. The relative normalization is arbitrary. The extra resonances in the CLYC, for example at 100 ns, are Cs resonances.

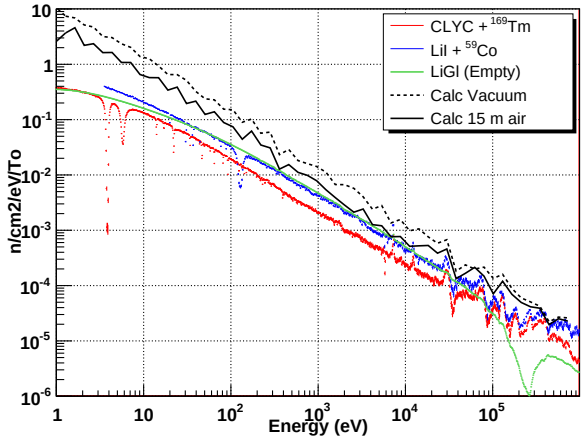

FIG. 11. Neutron flux at FP13 as measured by the CLYC, LiGl, and LiI detectors. The calculated flux for a fully evacuated flight path and one with the last 15 m in air is also shown.

energy range of interest. Representative calculations for several neutron energy ranges are shown in figures 12 to 16. Overall the measurements are in reasonable agreement with the calculations, but as the neutron energy increases, the resonance absorption dips in the calculated transmission are deeper than measured. This is just what is expected from increasing background at higher energies as shown in Figure 10.

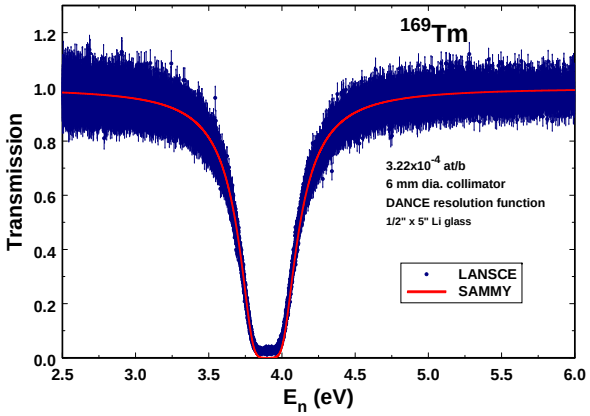

FIG. 12. Transmission for ^{169}Tm, measured in this experiment (blue points with statistical error bars) and calculated by SAMMY (red curve) for neutron energies from 2.5 to 6.0 eV

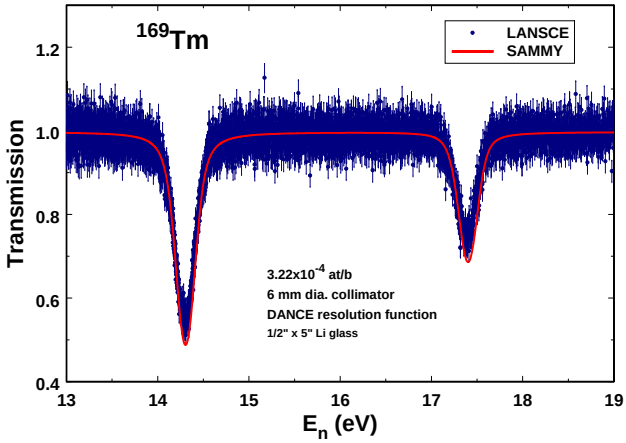

FIG. 13. Transmission for ^{169}Tm, measured in this experiment (blue points with statistical error bars) and calculated by SAMMY (red curve) for neutron energies from 13 to 19 eV

IV. ADDITIONAL PROGRESS IN FY16

Several tasks, in addition to data analysis, were completed after the test run in FY16.

1. The shielding over the first chopper in ER-1 was opened, and the chopper removed. A collimator was designed to go in the region between the FP13 external shutter and the beginning of the guide system. This will eliminate streaming paths in the shutter and around the neutron guides, as well as slightly reduce the amount of beam transported to the 30 m collimator. The collimator has been fabricated and installed. A lead filter will be added ahead of the 30 m collimator to reduce the gamma-ray background.

2. Dedicated detectors, data acquisition digitizers, and a computer have been procured. A 5 cm X 5 cm x 1 cm

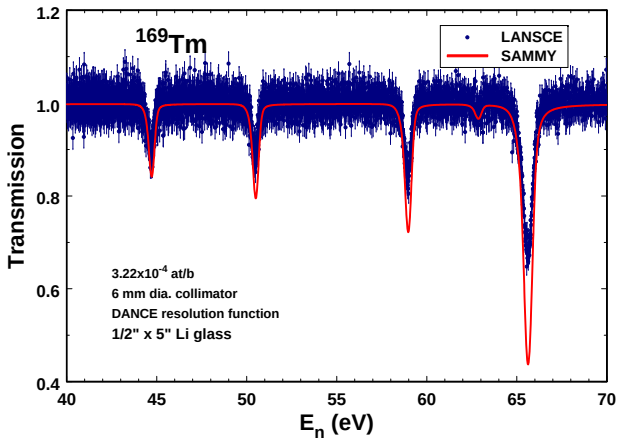

FIG. 14. Transmission for ^{169}Tm, measured in this experiment (blue points with statistical error bars) and calculated by SAMMY (red curve) for neutron energies from 40 to 70 eV

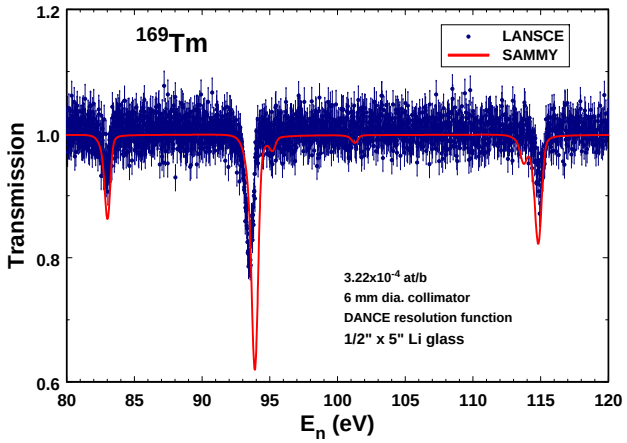

FIG. 15. Transmission for ^{169}Tm, measured in this experiment (blue points with statistical error bars) and calculated by SAMMY (red curve) for neutron energies from 80 to 120 eV

thick CLYC and similar size Li-glass crystal plus phototubes and gain-stabilized bases have been ordered. In addition the two Li-glass detectors used at ORNL for total cross section measurements at ORELA have been obtained.

3. Careful alignment of the flight path components is underway.

V. STEPS TO A PRODUCTION CAPABILITY

After FY16, several steps will still be needed to enable a production capability to measure total cross sections on small quantities of radioactive nuclides. These steps include the following.

1. Reduction of the gamma-ray backgrounds is the highest priority. The first step is installing a shielded beamstop and increasing the distance between the beam stop and the detector to minimize neutron and gamma return. The walls of the flight path around the detector should also be extended so that the detectors are not right against the polyethylene walls. Water-tight walls and roof in the detector region should also be constructed.

2. Backgrounds should be studied further using "black-resonance" samples with a range of resonance energies.

3. A complete measurement of resonance total cross sections on well-studied nuclides should be made to understand all the steps required to take and analyze the data to obtain final cross sections. These test measurements should include targets with high level density (such as ^{169}Tm) as well as low level density with well-resolved resonances to study the moderator resolution function. A sample-changing mechanism will be required to cycle sample-in/sample-out automatically on a few minute time scale. This will also require optimizing the data acquisition system and detectors.

4. Tests should be made with a low-mass sample of a well-studied stable nuclide to understand the challenges associated with aligning and measuring low-mass samples.

We note that the neutron guides in FP13 were very expensive to obtain, but are currently unused and unwanted, and may, in fact, be contributing to the gamma-ray and scattered-neutron background. They should be removed, and hopefully reused in another application.

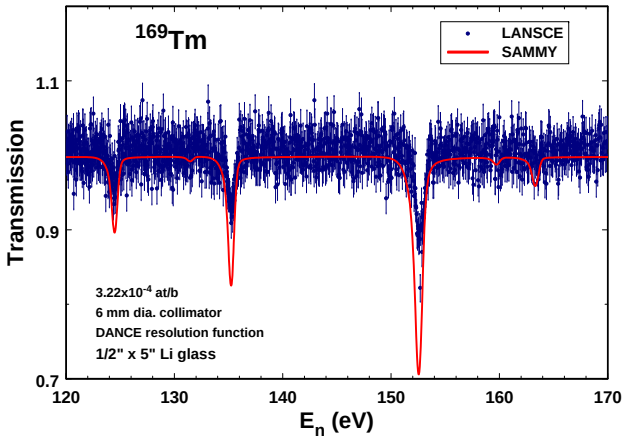

FIG. 16. Transmission for ^{169}Tm, measured in this experiment (blue points with statistical error bars) and calculated by SAMMY (red curve) for neutron energies from 120 to 170 eV

VI. CONCLUSIONS

During 2016, a great deal of progress was made in setting up the flight path and very promising preliminary

results were obtained. However, much work remains to be done to establish a production capability. The results of a simple test measurement of ^{169}Tm transmission were in good qualititative agreement with theoretical predictions using the SAMMY code, but a gamma-ray background was observed. Minimizing this background and optimizing detector performance will be the main goals for the next few months. Although challenges remain, we are quite optimistic that a world-class facility for total cross section measurements on very small quantities of target nuclides can be achieved.